

Electron-nuclear double resonance of interstitial chromium in silicon

R. van Kemp, E. G. Sieverts, and C. A. J. Ammerlaan

Natuurkundig Laboratorium der Universiteit van Amsterdam, Valckenierstraat 65, 1018 XE Amsterdam, The Netherlands

(Received 29 December 1986)

The positively charged state of interstitial chromium in silicon was investigated using electron-nuclear double resonance. We have found the hyperfine interaction of the impurity electrons with nine shells of surrounding silicon neighbors containing 102 atoms. The well-resolved fine structure due to the cubic-field splitting for chromium made it possible to determine the absolute signs of the measured hyperfine interaction parameters. The results are analyzed using a linear combination of atomic orbitals treatment that takes into account the spin $S = \frac{5}{2}$ of the impurity and the symmetry of the atomic orbitals centered at the ligands for the different shells. This analysis results in a spin density that is transferred from the impurity to the host crystal of at least 22%. The apparent contradiction between the reduced core polarization (indicating a delocalization of some 52% of the impurity wave function) and the absence of large hyperfine interactions with the silicon ligands is hereby resolved. Our results are compared with those obtained for the positively charged state of interstitial titanium and neutral interstitial iron. It appears that the electronic structure of chromium is similar to that of titanium.

I. INTRODUCTION

Chromium is one of the $3d$ transition-metal impurity atoms in silicon that was for the first time observed with electron paramagnetic resonance (EPR) by Woodbury and Ludwig.^{1,2} The other observed $3d$ transition metals were V, Mn, Fe, and Ni, sometimes in different charge states according to the n - or p -type doping level of the samples.³ A few years ago also the positively charged state of interstitial titanium was found.⁴

It is well established now that all the $3d$ transition metals diffuse interstitially and that Ti, V, Cr, Mn, and Fe occupy isolated interstitial sites upon quenching from high temperature.⁵

On the basis of their experiments, Ludwig and Woodbury developed a highly successful model to account for the observed effective spin and g values of the $3d$ transition metals in silicon. According to their model the introduction of a $3d$ metal on an interstitial site with tetrahedral symmetry causes a splitting of the atomic d levels in a threefold-degenerate t_2 and a twofold-degenerate e state (excluding spin); the e state lies higher in energy than the t_2 state. These levels are filled according to Hund's rule. Finally, the $4s$ electrons are not used for bonding to the silicon nearest neighbors, and are transferred to the $3d$ shell.

For Cr_i^+ , which has the configuration $3d^5$, this leads to a $t_2^3 e^2$ (6A_1) state. The existence of a donor level has been proved by EPR observations of Cr_i^0 and Cr_i^+ , Hall effect, resistivity measurements,^{1,6} and with deep-level transient spectroscopy (DLTS).⁷ From these experiments the donor level $\text{Cr}_i^{0/+}$ was established to lie at $E_c - 0.22$ eV.

The EPR data of Ludwig and Woodbury immediately posed a contradiction. The observed hyperfine interaction between the $3d$ electrons and the impurity nucleus is smaller than was calculated for the free Cr_i^+ ion.⁸

From this reduction a rather large delocalization of the $3d$ wave functions, resulting in large hyperfine interactions with the silicon ligands, would be expected. However, no large hyperfine interactions are resolved in EPR. Since a few years ago, there has been a renewed interest in this problem both from theoretical⁹⁻¹⁴ and experimental points of view.¹⁵⁻¹⁷

We have performed electron-nuclear double-resonance (ENDOR) experiments in silicon containing Cr_i^+ , resolving the hyperfine interaction between the impurity electrons and 102 silicon atoms in nine shells surrounding the chromium.

In Sec. II we will give an outline of the experimental procedure; in Sec. III the experimental results are presented, which are discussed in Sec. IV. Conclusions are summarized in Sec. V.

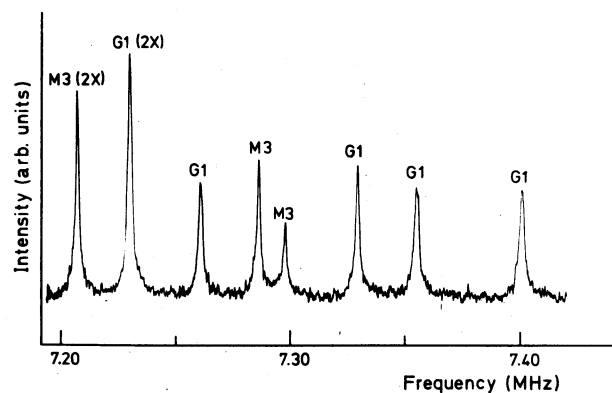


FIG. 1. Recorder trace of an ENDOR spectrum. The magnetic field is $B = 826.830$ mT and is parallel to $[110]$. The microwave frequency was 23.1239 GHz. Shown are resonances for the interaction tensors G1 and M3. The resonances are arising from NMR transitions between the levels $|-\frac{1}{2}, +\frac{1}{2}\rangle$ and $|-\frac{1}{2}, -\frac{1}{2}\rangle$, observed on EPR transition $|+\frac{1}{2}\rangle \leftrightarrow |-\frac{1}{2}\rangle$.

II. EXPERIMENTAL PROCEDURE

Samples containing Cr_i^+ were prepared by coating silicon bars (dimensions $2 \times 2 \times 20 \text{ mm}^3$) doped with boron ($[\text{B}] \sim 0.8 \times 10^{16} - 1.8 \times 10^{16} \text{ atoms cm}^{-3}$), aluminum ($[\text{Al}] \sim 2 \times 10^{16} \text{ atoms cm}^{-3}$), or gallium ($[\text{Ga}] \sim 1.0 \times 10^{16} \text{ atoms cm}^{-3}$) with solutions of CrO_3 or CrCl_3 . These samples were heated in an evacuated quartz ampoule for 24 h at 1350°C and subsequently quenched. The intensity of the Cr_i^+ EPR spectrum was found to be the same for all three acceptor dopants.

The EPR and ENDOR measurements were done in a

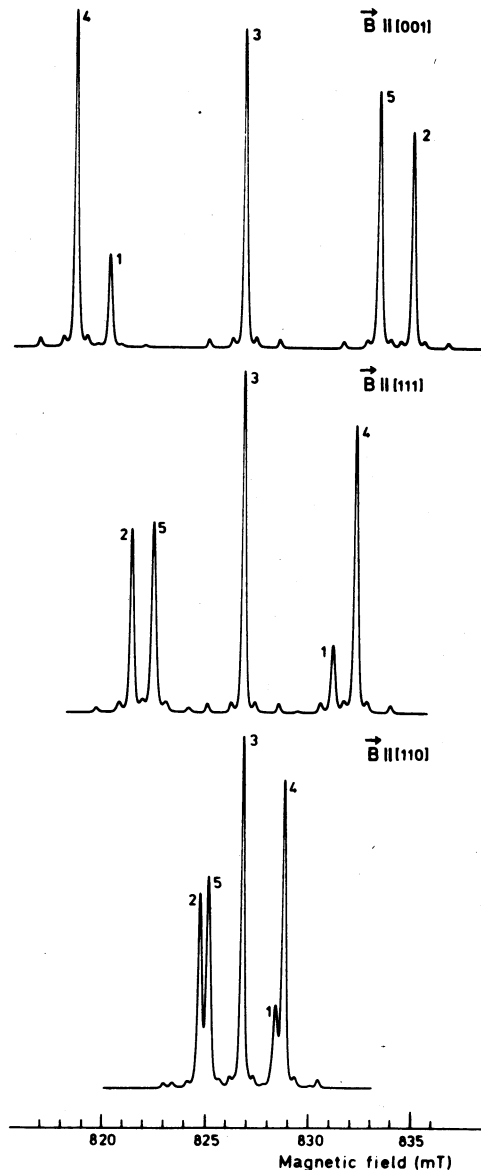


FIG. 2. EPR spectra for the three directions of high symmetry in the $(\bar{1}10)$ plane: $[001]$, $[111]$, and $[110]$. The spectra show a fine structure due to the cubic field splitting. The microwave frequency was 23.1244 GHz. The EPR lines are labeled according to the EPR transitions: $1 = | +\frac{5}{2} \rangle \leftrightarrow | +\frac{3}{2} \rangle$, $2 = | +\frac{3}{2} \rangle \leftrightarrow | +\frac{1}{2} \rangle$, $3 = | +\frac{1}{2} \rangle \leftrightarrow | -\frac{1}{2} \rangle$, $4 = | -\frac{1}{2} \rangle \leftrightarrow | -\frac{3}{2} \rangle$, and $5 = | -\frac{3}{2} \rangle \leftrightarrow | -\frac{5}{2} \rangle$. Centered around each EPR line four hyperfine lines are visible which are due to the 9.54% abundant magnetic isotope ^{53}Cr , which has nuclear spin $I = \frac{3}{2}$.

superheterodyne spectrometer operating at 23 GHz. A cylindrical TE_{011} cavity made of Epibond was used; the inner wall of this cavity was covered with a thin layer of silver in which a groove was cut, enabling the wall to act as a coil for radio frequencies.¹ Nuclear magnetic resonances were recorded as changes in the dispersion component of the EPR signal using double phase-sensitive detection by modulating the magnetic field with 83.3 Hz and the radio frequencies with 3.3 Hz. The magnetic field could be rotated in a $\{110\}$ plane of the crystal. The experiment was performed with the sample at liquid-helium temperature, 4.2 K. Figure 1 shows a typical recorder trace of an ENDOR spectrum.

III. EXPERIMENTAL RESULTS

The EPR and ligand ENDOR spectra of Si:Cr_i^+ can be described using the effective spin Hamiltonian

$$\mathcal{H} = g\mu_B \mathbf{B} \cdot \mathbf{S} + \frac{1}{6}a[S_x^4 + S_y^4 + S_z^4 - \frac{1}{5}S(S+1)(3S^2 + 3S - 1)] + \sum_i (\mathbf{S} \cdot \vec{A}_i \cdot \mathbf{I}_i - g_N \mu_N \mathbf{B} \cdot \mathbf{I}_i), \quad (1)$$

with $S = \frac{5}{2}$ and $I = \frac{1}{2}$. The first term accounts for the Zeeman interaction between the impurity electrons and the magnetic field, the second term is the cubic field splitting, the third term is the interaction between the impurity electrons and a ^{29}Si nucleus, and the last term accounts for the nuclear Zeeman interaction. In Fig. 2 the EPR spectra in three directions of high symmetry are shown. Centered around each EPR line four hyperfine lines are visible which are due to the 9.54% abundant magnetic isotope ^{53}Cr , which has nuclear spin $I = \frac{3}{2}$. Due to the cubic field term, which is resolved in EPR, each spectrum consists of $2S$ fine-structure lines. The intensities of these lines are not equal as a result of different transition probabilities and different popula-

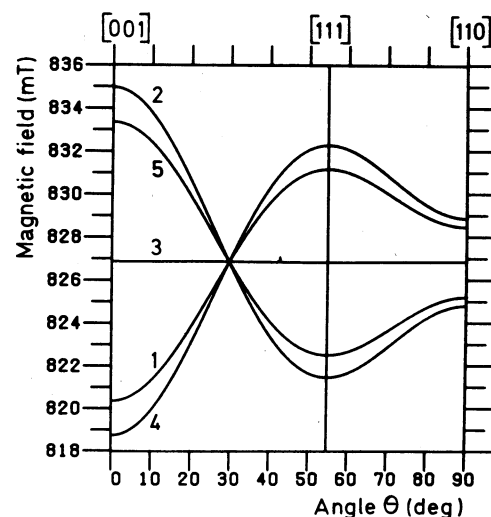


FIG. 3. Angular dependence of the Si:Cr_i^+ spectrum for rotation of the magnetic field in the $(\bar{1}10)$ plane. The lines are labeled according to the EPR transitions: $1 = | +\frac{5}{2} \rangle \leftrightarrow | +\frac{3}{2} \rangle$, $2 = | +\frac{3}{2} \rangle \leftrightarrow | +\frac{1}{2} \rangle$, $3 = | +\frac{1}{2} \rangle \leftrightarrow | -\frac{1}{2} \rangle$, $4 = | -\frac{1}{2} \rangle \leftrightarrow | -\frac{3}{2} \rangle$, and $5 = | -\frac{3}{2} \rangle \leftrightarrow | -\frac{5}{2} \rangle$.

tions of these levels. From the intensities and the changes of intensities with temperature, one is able to label each line with the m_S quantum numbers. A plot of the positions of the different fine-structure lines upon rotation of the magnetic field is shown in Fig. 3. In the labeling as used in Figs. 2 and 3, lines 1–5 belong to the transitions $|+\frac{5}{2}\rangle \leftrightarrow |+\frac{3}{2}\rangle$, $|+\frac{3}{2}\rangle \leftrightarrow |+\frac{1}{2}\rangle$, $|+\frac{1}{2}\rangle \leftrightarrow |-\frac{1}{2}\rangle$, $|-\frac{1}{2}\rangle \leftrightarrow |-\frac{3}{2}\rangle$, and $|-\frac{3}{2}\rangle \leftrightarrow |-\frac{5}{2}\rangle$, respectively. In these assignments the sign of the electronic g factor was assumed to be positive.¹⁸

Each atomic site around a chromium atom at the tetrahedral interstitial site has a 4.7% probability of being occupied by a ^{29}Si nucleus with nuclear spin $I = \frac{1}{2}$. By applying the symmetry operations of the $\bar{4}3m$ (T_d) point group on such a ^{29}Si atom in the crystal, a shell of symmetry-related sites is generated. In general, such a shell will contain 24 atoms, giving rise to an ENDOR spectrum of 2×24 lines for an arbitrary direction of the magnetic field \mathbf{B} . Because we rotate the magnetic field in the $(\bar{1}10)$ plane of the crystal, only 2×12 lines will be

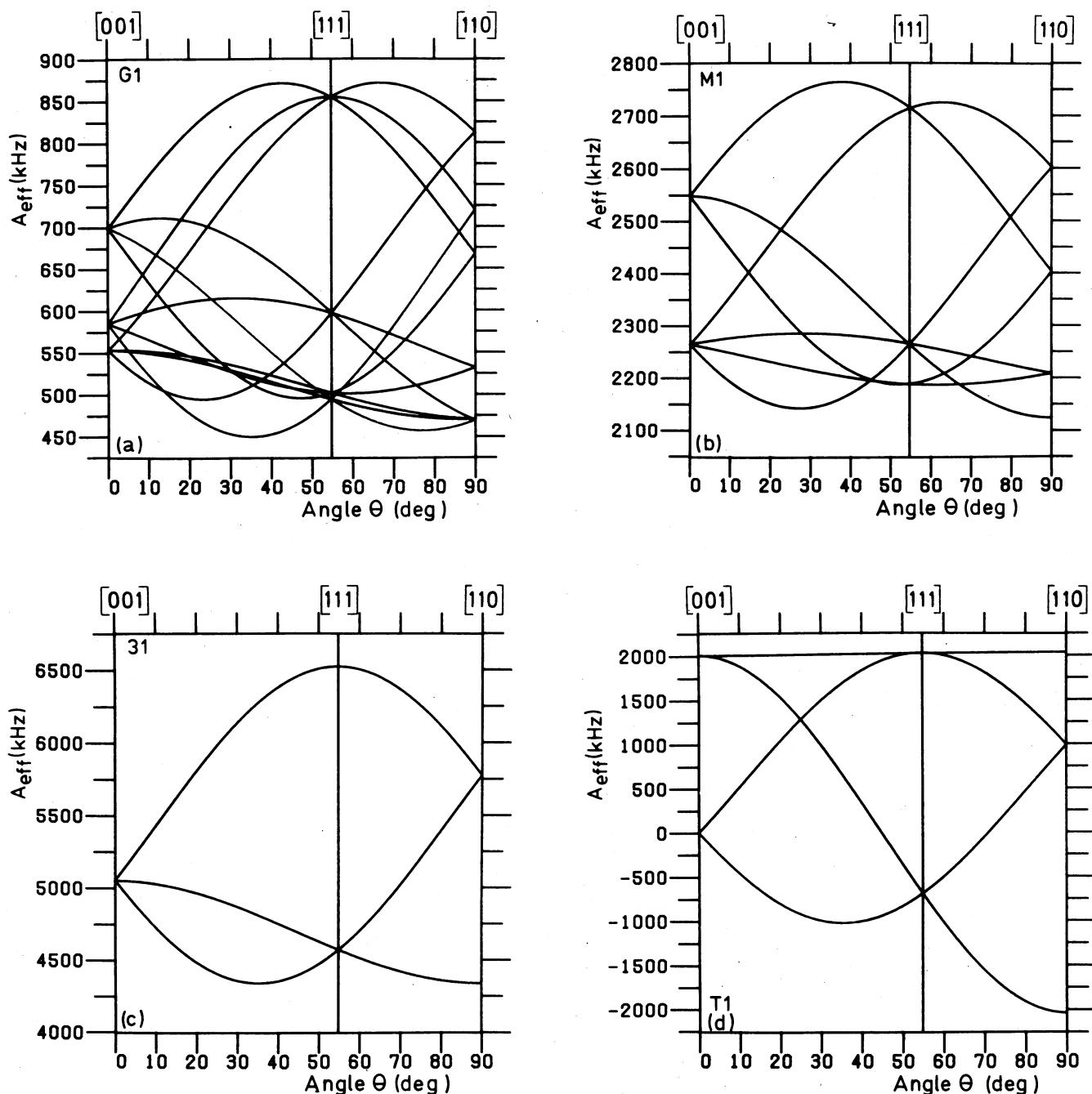


FIG. 4. (a) Angular dependence of the general-class hyperfine-interaction tensor with the largest isotropic part, G1. (b) Angular dependence of the mirror-plane-class hyperfine-interaction tensor with the largest isotropic part, M1. (c) Angular dependence of the class-3 hyperfine-interaction tensor with the largest isotropic part, 31. (d) Angular dependence of the class-2mm hyperfine-interaction tensor, T1.

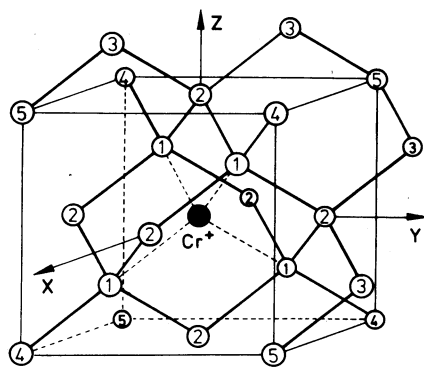


FIG. 5. The position of Cr_i^+ (solid sphere) in the silicon crystal. All hyperfine-interaction tensors in Table I are given in this coordinate system.

observed. The angular dependence of a single set of 12 ENDOR lines originating from such a shell is shown in Fig. 4(a). In the experiment hyperfine interactions with two such shells, labeled G1 and G2, were observed. If the ^{29}Si nucleus is lying in a $\{110\}$ mirror plane, the shell in this class contains 12 atoms. An example of the angular dependence for such a shell is shown in Fig. 4(b). Three such shells, labeled M1–M3, were found. The atoms labeled 3 in Fig. 5 form part of such a shell. When the ^{29}Si nucleus is lying on a $\langle 111 \rangle$ axis, a shell contains four atoms. In Fig. 4(c) an angle-dependent pattern for such a shell is shown; in Fig. 5 the atoms in three of these shells are labeled 1, 4, and 5. Three shells of this type were found, with labels 31–33. Finally, there are also silicon atoms that lie on a twofold rotation axis through the impurity atom. These atoms form shells containing six atoms. The interaction with only one such shell was found [Fig. 4(d)]; in Fig. 5 the sites for the nearest-neighbor shell in this class are labeled 2. In total, the nine shells contain $2 \times 24 + 3 \times 12 + 3 \times 4 + 1 \times 6 = 102$ atoms.

Before starting the ENDOR experiments we made a computer fit of our EPR measurements to the spin Hamiltonian given in Eq. (1), omitting the nuclear terms from it. We found that $g = 1.9982 \pm 0.0001$ and $a/h = 90.9 \pm 0.1$ MHz. Ludwig and Woodbury gave, respec-

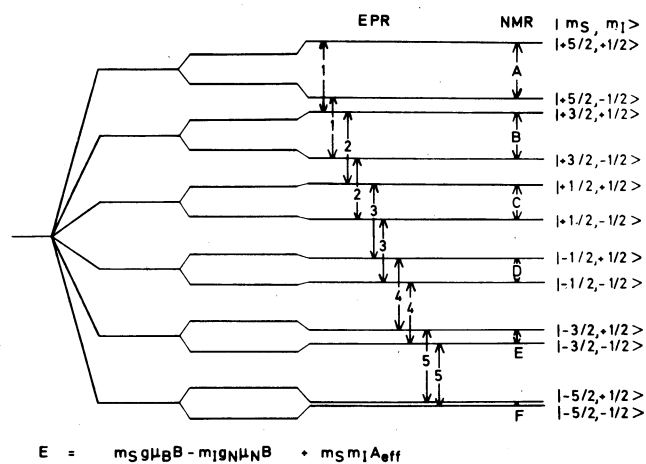


FIG. 6. Schematic level diagram for the $\text{Si}:\text{Cr}_i^+$ spin system with $S = \frac{5}{2}$ and $I = \frac{1}{2}$. EPR transitions are indicated 1–5, NMR transitions are indicated A–F. The ordering of the levels corresponds to $g > 0$, $g_N < 0$, and $A_{\text{eff}} > 0$.

tively, $g = 1.9978$ and $a/h = 90.42$ MHz. The discrepancies are outside the quoted error margins. Our values were calculated by computer diagonalization of the spin Hamiltonian, while Ludwig and Woodbury used perturbation theory.

Because the EPR spectrum of chromium has a fine structure due to the cubic field splitting, it was possible to determine the absolute sign of the hyperfine interactions. To first order and neglecting the cubic field splitting, possible NMR transitions are at

$$\nu = \nu_z + m_S A_{\text{eff}}/h \quad (m_S = -\frac{5}{2}, \dots, +\frac{5}{2}), \quad (2)$$

where $\nu_z = -g_N \mu_N B/h$ is the nuclear Zeeman frequency and A_{eff} is the effective hyperfine interaction. Since the ENDOR mechanism is based on spin-relaxation processes, the intensity of an EPR transition between two levels will be affected more by NMR transitions between levels that are coincident with the levels involved in the EPR than by those NMR transitions that are not (directly) coupled. This is schematically depicted in Fig. 6, where we show a simplified level scheme for an $S = \frac{5}{2}$ and $I = \frac{1}{2}$ spin system. For instance, it is expected that the intensity of the EPR transitions labeled 2

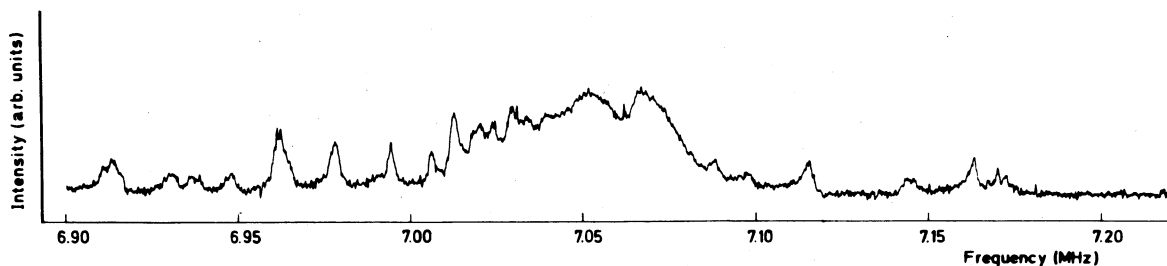


FIG. 7. Recorder trace of an ENDOR scan around the nuclear Zeeman frequency $\nu_z = 7.060$ MHz with the magnetic field $B = 834.65$ mT $\parallel [001]$. The ENDOR lines are due to the transitions $|+\frac{3}{2}, +\frac{1}{2}\rangle \leftrightarrow |+\frac{3}{2}, -\frac{1}{2}\rangle$, transition B in Fig. 6, and $|+\frac{1}{2}, +\frac{1}{2}\rangle \leftrightarrow |+\frac{1}{2}, -\frac{1}{2}\rangle$, transition C in Fig. 6. Most lines including a large unresolved cluster show below the nuclear Zeeman frequency, only few lines above ν_z . The former lines correspond to $A_{\text{eff}} < 0$, the latter to $A_{\text{eff}} > 0$.

TABLE I. Hyperfine parameters of interstitial chromium in silicon. Units of \vec{A} (Cartesian tensor) and A_i (principal values) are in kHz. \hat{n}_i gives the direction of the i th principal value of \vec{A} . The experimental error is ± 0.5 kHz, except for the tensors 31 and 32, where it is ± 1 kHz.

Class	m_S	\vec{A}			i	A_i	\hat{n}_i		
G1	$+\frac{1}{2}, -\frac{1}{2}$	-699.4	-171.0	94.1	1	-449.7	[0.402	-0.816	-0.416]
		-171.0	-584.7	99.2	2	-509.2	[0.545	-0.152	0.824]
		94.1	99.2	-553.2	3	-878.0	[0.736	0.558	-0.384]
G2	$+\frac{1}{2}, -\frac{1}{2}$	-168.1	-28.8	59.4	1	-118.5	[0.587	-0.804	0.100]
		-28.8	-135.4	33.3	2	-124.0	[0.566	0.495	0.660]
		59.4	33.3	-199.9	3	-260.9	[0.579	0.331	-0.745]
M1	$+\frac{1}{2}, -\frac{1}{2}$	-2264.5	-140.1	-196.8	1	-2124.5	[0.707	-0.707	0.000]
		-140.1	-2264.5	-196.8	2	-2763.9	[0.433	0.433	0.791]
		-196.8	-196.8	-2548.4	3	-2189.1	[0.559	0.559	-0.612]
M2	$+\frac{1}{2}, -\frac{1}{2}$	-1424.3	-214.2	-84.7	1	-1210.0	[0.707	-0.707	0.000]
		-214.2	-1424.3	-84.7	2	-1677.9	[0.672	0.672	0.313]
		-84.7	-84.7	-1314.0	3	-1274.6	[0.221	0.221	-0.950]
M3	$+\frac{1}{2}, -\frac{1}{2}$	-514.8	-91.0	-79.6	1	-423.8	[0.707	-0.707	0.000]
		-91.0	-514.8	-79.6	2	-674.9	[0.603	0.603	0.523]
		-79.6	-79.6	-491.2	3	-422.1	[0.370	0.370	-0.853]
31	$-\frac{1}{2}$	-5067.4	-727.7	-727.7	1	-6522.7	[0.577	0.577	0.577]
		-727.7	-5067.4	-727.7	2	-4339.7	[0.707	-0.707	0.000]
		-727.7	-727.7	-5067.4	3	-4339.7	[0.408	0.408	-0.816]
32	$-\frac{1}{2}$	-3269.3	-332.3	-332.3	1	-3934.0	[0.577	0.577	0.577]
		-332.3	-3269.3	-332.3	2	-2937.0	[0.707	-0.707	0.000]
		-332.3	-332.3	-3269.3	3	-2937.0	[0.408	0.408	-0.816]
33	$+\frac{1}{2}$	216.7	-109.6	-109.6	1	-2.4	[0.577	0.577	0.577]
		-109.6	216.7	-109.6	2	326.3	[0.707	-0.707	0.000]
		-109.6	-109.6	216.7	3	326.3	[0.408	0.408	-0.816]
T1	$+\frac{1}{2}, -\frac{1}{2}$	1.0	-2036.6	0	1	2037.6	[0.707	-0.707	0.000]
		-2036.6	1.0	0	2	-2035.6	[0.707	0.707	0.000]
		0	0	2002.9	3	2002.9	[0.000	0.000	1.000]

($m_S = |+\frac{3}{2}\rangle \leftrightarrow |+\frac{1}{2}\rangle$) will change only if the NMR transitions labeled *B* and *C* are induced. This was verified experimentally by setting the magnetic field on the EPR line belonging to the transitions labeled 2 in Fig. 6 and scanning the radio frequencies around the Zeeman frequency. This frequency lies at about 7 MHz for a magnetic field of about 825 mT. On EPR transition 2 only NMR frequencies at

$$\nu = \nu_z + \frac{1}{2} A_{\text{eff}}/h \quad \text{and} \quad \nu = \nu_z + \frac{3}{2} A_{\text{eff}}/h \quad (3)$$

are found. In this way the sign of A_{eff} is determined. The ENDOR lines for most shells for this EPR transition were found to lie at frequencies lower than ν_z , indicating that $A_{\text{eff}} < 0$ for the corresponding tensors. The two exceptions were the tensors T1 and 33, for which A_{eff} is positive for most directions of the magnetic field. In Fig. 7 an ENDOR scan around the nuclear Zeeman

frequency is shown with the magnetic field set to the EPR line labeled 2 in Fig. 6.

Angle-dependent ENDOR scans were made for the EPR transition labeled 3 and the NMR transitions labeled *C* in Fig. 6; for the NMR transitions labeled *D* only scans were made in the [001], [111], and [110] directions, except for the tensors 31, 32, and 33. When making computer fits to the hyperfine tensors, the electron g value, the cubic field splitting parameter a , and g_N were kept constant. The latter constant was determined first by making a simultaneous fit to the observed ENDOR frequencies belonging to $m_S = \frac{1}{2}$ and $-\frac{1}{2}$ for all the tensors, except 31, 32, and 33. The value thus found was $g_N = -1.1098$, in close agreement with literature.¹⁹ The results of our measurements are given in Table I, where also the NMR transitions are indicated that were used in the computer fits. The tensors and directions of

the eigenvectors in this table are defined in the coordinate system of Fig. 5 and are valid for the following.

- (1) The atom on the [111] axis for shells 31–33.
- (2) One of the two atoms on the [001] axis for the T1 shell, since no unique assignment of the hyperfine tensor to one of these atoms can be made.
- (3) One of the two atoms (for the same reasons as in 2) in the $(\bar{1}10)$ mirror plane for shells M1–M3.
- (4) One of the 24 atoms in the shells with the lowest symmetry, G1 and G2.

Typical ENDOR linewidths were on the order of 4 kHz full width at half maximum, except for the tensors 31 and 32, where the widths were about 8 kHz. The accuracy for the fits is on the order of 0.5 and 1 kHz, respectively.

IV. DISCUSSION

Since all transition-metal $4s$ electrons are supposed to be transferred to $3d$ orbitals, the isotropic impurity hyperfine interaction must originate from core polarization. The magnitude of the core polarization tends to be approximately proportional to the amount of polarizing d orbitals. As mentioned in the Introduction, the reduction of the hyperfine field at the impurity therefore suggests a considerable delocalization of the wave function. In principle, this should lead to strong hyperfine interactions with the ligand nuclei.

In a comparable case, Fe_i^0 , a reduction by some 52% can be calculated when comparing the experimental value of the hyperfine field to values calculated for the exchange polarization by Freeman and Watson.⁸ The spin delocalization as calculated from ENDOR experiments, however, was originally on the order of only 5% (under less realistic assumptions, at most 20%).¹⁵ A more recent analysis yielded a 25% spin density on the ligand atoms,¹⁷ in better agreement with theoretical data.¹¹ Another similar system is Ti_i^+ in silicon. Here one calculates a reduction by 74% for the central-atom hyperfine interaction.¹⁶ From ligand hyperfine interactions only about 34% delocalization is found in the one-electron linear combination of atomic orbitals (LCAO) approximation as used by Watkins and Corbett.²⁰ A more sophisticated analysis yielded in this case only a lower limit. A minimum spin transfer of 40% to the silicon lattice was found.¹⁶

For chromium, using the value of the impurity hyperfine field as given by Watson and Freeman,⁸ a net spin density for the free ion of $|\Psi(0)|^2 = 8.87 \times 10^{-30} \text{ m}^{-3}$ follows. From the experimental data given by Woodbury and Ludwig, $A/h = 31.99 \text{ MHz}$,¹ and using

$$A = \frac{1}{2S} \frac{2}{3} \mu_0 g \mu_B g_N \mu_N |\Psi(0)|^2, \quad (4)$$

one calculates $|\Psi(0)|^2 = 4.28 \times 10^{30} \text{ m}^{-3}$ for Cr_i^+ in silicon. Compared to the free ion the hyperfine field is reduced by 52%. Analyzing the present data using the one-electron LCAO approach, one finds a delocalization of 22%.

It is understandable that the one-electron LCAO ap-

proximation is not suited for a system where the paramagnetism arises from several unpaired d electrons. As was shown for Ti_i^+ , better results can be obtained by taking into account the proper more-electron wave function of the impurity atom and the ligand orbitals that have the correct symmetry with regard to the point-

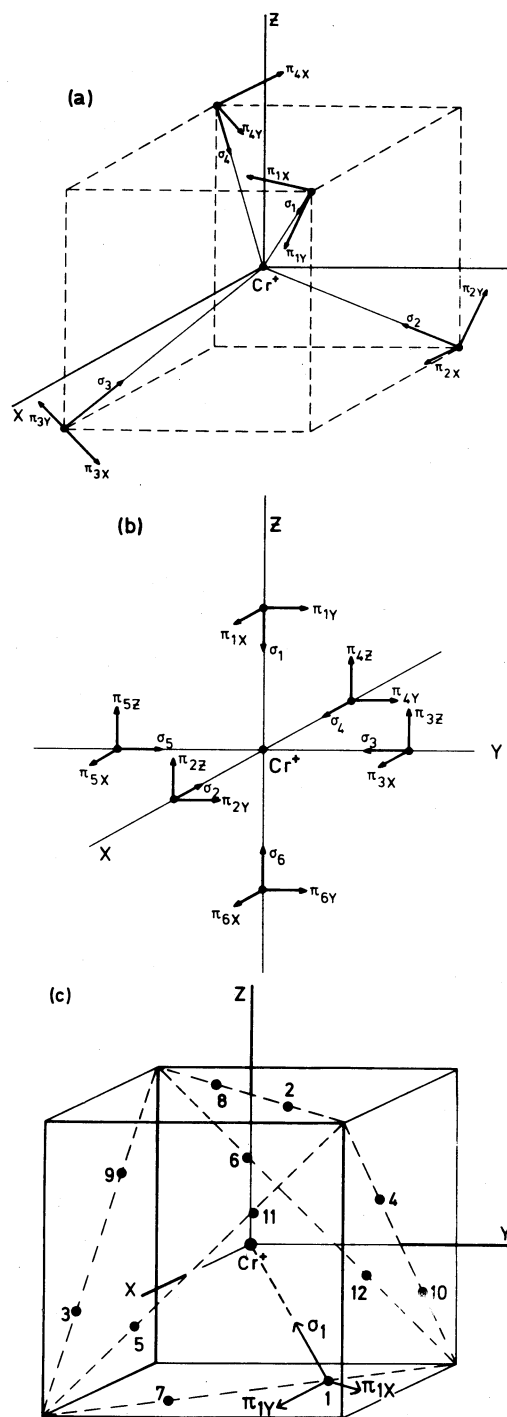


FIG. 8. (a) Orientations of the σ and π orbitals centered on the atoms of a class-3 shell. (b) Orientations of the σ and π orbitals centered on the atoms of a class-2mm shell. (c) Orientations of the σ and π orbitals centered on the atoms of a class-M shell. The numbers 1–12 refer to the positions $\bar{m}m\bar{n}$, mmn , $m\bar{n}\bar{m}$, $m\bar{m}\bar{n}$, $m\bar{m}n$, $\bar{m}m\bar{n}$, $\bar{m}m\bar{n}$, $\bar{m}m\bar{n}$, $\bar{m}m\bar{n}$, mmn , and $\bar{m}m\bar{m}$. The π_{1x} and π_{1y} orbitals are along [110] and $[n\bar{n}2\bar{m}]$, respectively.

group symmetry of the interstitial T_d site in the crystal. A review of this method is given by Owen and Thornley,²¹ who apply it to the effects of covalent bonding on the magnetic properties of octahedrally coordinated ions with an unfilled d shell. We have analyzed our data using this same procedure for the various possible neighbor coordinations in the silicon lattice.

The experimental hyperfine interaction tensors \vec{A}_i are usually split into two parts, $\vec{A}_i = a_i \vec{1} + \vec{B}_i$, where $a_i = \frac{1}{3} \text{Tr}(\vec{A}_i)$ is the isotropic part and \vec{B}_i is a traceless tensor describing the anisotropic part of \vec{A}_i . The isotropic part is related to the Fermi-contact interaction by

$$a_i = \frac{1}{2S} \frac{2}{3} \mu_0 g \mu_B g_N \mu_N |\Psi(0)|_i^2, \quad (5)$$

where $|\Psi(0)|_i^2$ is the probability of finding the unpaired electrons at nucleus i . As $g_N < 0$ and all the other constants in Eq. (5) are positive, it is expected that $a_i < 0$. In some cases, as we will see, positive values of a_i are found in the experiment. The tensor \vec{B}_i , which represents the anisotropic part of \vec{A}_i , is the dipole-dipole interaction tensor given by

$$B_{ij} = \frac{1}{2S} \frac{\mu_0}{4\pi} g \mu_B g_N \mu_N \left\langle \Psi \left| \frac{3x_i x_j}{r^5} - \frac{\delta_{ij}}{r^3} \right| \Psi \right\rangle, \quad (6)$$

where Ψ is the electron wave function and $x_i, x_j = x, y, z$ with respect to a particular site.

Following the procedure as outlined by Owen and Thornley, we write the wave functions as a $3d$ orbital on the Cr ion to which a combination of $3s$ and $3p$ orbitals on silicon atoms is admixed. The p orbitals are chosen as one σ and two π orbitals on each silicon atom. The σ orbital is pointing towards the impurity ion and the two π orbitals are perpendicular to each other and to the σ orbital. Using projection operators we calculated the properly symmetrized linear combinations of σ and π orbitals for each of the four symmetry types of neighbor atoms.

In the Ludwig-Woodbury model the ground state of Cr_i^+ is $t_2^2 e^2$ and the wave function can be written as a single determinant $\{\Psi_{xy} \Psi_{yz} \Psi_{zx} \Psi_{x^2-y^2} \Psi_{3z^2-r^2}\}$ because the orbital magnetic moment is quenched. We may thus add up the separate contributions to the hyperfine interaction from the singly occupied orbitals.

For the class-3 shells the choice of the ligand σ and π orbitals is shown in Fig. 8(a); σ_k ($k=1-4$) is along a $\langle 111 \rangle$ direction and π_{kx} and π_{ky} are along $\langle 211 \rangle$ and $\langle 011 \rangle$ directions, respectively. For the class-3 shells it follows that

$$\begin{aligned} \Psi_{yz} &= a d_{yz} + \frac{1}{2} \beta_i (s_1 - s_2 + s_3 - s_4) + \frac{1}{2} \gamma_i (\sigma_1 - \sigma_2 + \sigma_3 - \sigma_4) + \frac{1}{4} \delta_i [(-\pi_{1x} + \pi_{2x} - \pi_{3x} + \pi_{4x}) \\ &\quad + \sqrt{3}(-\pi_{1y} + \pi_{2y} - \pi_{3y} + \pi_{4y})], \\ \Psi_{zx} &= a d_{zx} + \frac{1}{2} \beta_i (s_1 + s_2 - s_3 - s_4) + \frac{1}{2} \gamma_i (\sigma_1 + \sigma_2 - \sigma_3 - \sigma_4) + \frac{1}{2} \delta_i (\pi_{1x} + \pi_{2x} - \pi_{3x} - \pi_{4x}), \\ \Psi_{xy} &= a d_{xy} + \frac{1}{2} \beta_i (s_1 - s_2 - s_3 + s_4) + \frac{1}{2} \gamma_i (\sigma_1 - \sigma_2 - \sigma_3 + \sigma_4) + \frac{1}{4} \delta_i [(-\pi_{1x} + \pi_{2x} + \pi_{3x} - \pi_{4x}) \\ &\quad + \sqrt{3}(\pi_{1y} - \pi_{2y} - \pi_{3y} + \pi_{4y})], \\ \Psi_{x^2-y^2} &= a' d_{x^2-y^2} + \frac{1}{4} \epsilon_i [\sqrt{3}(\pi_{1x} + \pi_{2x} + \pi_{3x} + \pi_{4x}) + (\pi_{1y} + \pi_{2y} + \pi_{3y} + \pi_{4y})], \\ \Psi_{3z^2-r^2} &= a' d_{3z^2-r^2} + \frac{1}{4} \epsilon_i [(\pi_{1x} + \pi_{2x} + \pi_{3x} + \pi_{4x}) - \sqrt{3}(\pi_{1y} + \pi_{2y} + \pi_{3y} + \pi_{4y})]. \end{aligned} \quad (7)$$

With the expressions (5) and (6) and using these five LCAO wave functions, the Fermi-contact interaction and the anisotropic hyperfine interaction can be calculated. In calculating hyperfine tensors for a specific site, we neglect contributions from the wave functions on other sites, except for the dipole-dipole contribution due to the impurity d orbitals, which are considered distant point charges. For the Fermi-contact interaction we calculated

$$a_i = \frac{1}{2S} \frac{2}{3} \beta_i^2 \frac{2}{3} \mu_0 g \mu_B g_N \mu_N |s(0)|^2. \quad (8)$$

For the dipole-dipole interaction tensor in the $\pi_x \pi_y \sigma$ coordinate system, it was calculated that

$$\begin{aligned} B_{\xi\xi} &= B_{\eta\eta} = \frac{1}{2S} \left[-\frac{3}{4} \gamma_i^2 + \frac{3}{8} (\delta_i^2 + \frac{2}{3} \epsilon_i^2) \right] b \\ &\quad - \frac{1}{2S} (3\alpha^2 + 2\alpha'^2) b_{dd}, \\ B_{\xi\xi} &= -B_{\xi\xi} - B_{\eta\eta}, \\ B_{\xi\eta} &= B_{\eta\xi} = B_{\eta\xi} = B_{\xi\eta} = B_{\xi\xi} = B_{\xi\xi} = 0, \end{aligned} \quad (9)$$

with

$$b = \frac{2}{5} \frac{\mu_0}{4\pi} g \mu_B g_N \mu_N \langle r^{-3} \rangle_p$$

and

$$b_{dd} = \frac{\mu_0}{4\pi} g \mu_B g_N \mu_N R^{-3},$$

where R is the distance between the impurity and the ligand atom. The atomic parameters used in the numerical analysis are $|s(0)|^2 = 34.52 \times 10^{30} \text{ m}^{-3}$ (5.115 a.u.⁻³) and $\langle r^{-3} \rangle_p = 18.16 \times 10^{30} \text{ m}^{-3}$ (2.691 a.u.⁻³).²²

As can be seen from Eqs. (8) and (9), it is not possible to calculate $\frac{3}{5}(\beta_i^2 + \gamma_i^2 + \delta_i^2) + \frac{2}{5}\epsilon_i^2$, the transferred spin density to shell i ; it is only possible to calculate the quantities β_i^2 and $\frac{3}{4}\gamma_i^2 - \frac{3}{8}(\delta_i^2 + \frac{2}{3}\epsilon_i^2)$ for the experimental tensors as a function of $\frac{3}{5}\alpha^2 + \frac{2}{5}\alpha'^2$. As contributions from σ and π orbitals are found to counteract, only a minimum value of the transferred spin density (MTSD) can be deduced. In this procedure we set, for instance,

$$B_{\xi\xi} = -\frac{1}{2S} \frac{3}{4} \gamma_i^2 b$$

when $B_{\xi\xi} > 0$ and

$$B_{\xi\xi} = \frac{1}{2S} \frac{3}{8} \delta_i^2 b \quad \text{or} \quad B_{\xi\xi} = \frac{1}{2S} \frac{1}{4} \epsilon_i^2 b$$

when $B_{\xi\xi} < 0$. It is also seen that it is impossible to discriminate between contributions from the t_2 and e states. The contributions from the π orbitals will be the

same irrespective of whether δ_i^2 is taken zero and ϵ_i^2 is calculated or vice versa. The factor $\frac{2}{3}$ for ϵ_i^2 results also in the factor $\frac{3}{5}$, just as for δ_i^2 . As will be seen, this factor $\frac{2}{3}$ is found for every coefficient occurring in the e -state wave functions. Still it is possible to set a lower limit to the value of spin density that is transferred to the crystal.

In the same manner as for the class-3 shell tensors, the following expressions for the class-2 mm shell tensor were obtained:

$$\begin{aligned} \Psi_{yz} &= ad_{yz} + \frac{1}{\sqrt{2}} \beta_i (s_2 - s_4) + \frac{1}{\sqrt{2}} \gamma_i (\sigma_2 - \sigma_4) + \frac{1}{2} \delta_i (\pi_{1x} + \pi_{3x} + \pi_{5x} + \pi_{6x}) + \frac{1}{2} \epsilon_i (\pi_{1y} + \pi_{3z} - \pi_{5z} - \pi_{6y}), \\ \Psi_{zx} &= ad_{zx} + \frac{1}{\sqrt{2}} \beta_i (s_3 - s_5) + \frac{1}{\sqrt{2}} \gamma_i (\sigma_3 - \sigma_5) + \frac{1}{2} \delta_i (\pi_{1y} + \pi_{2y} + \pi_{4y} + \pi_{6y}) + \frac{1}{2} \epsilon_i (\pi_{1x} + \pi_{2z} - \pi_{4z} - \pi_{6x}), \\ \Psi_{xy} &= ad_{xy} + \frac{1}{\sqrt{2}} \beta_i (s_1 - s_6) + \frac{1}{\sqrt{2}} \gamma_i (\sigma_1 - \sigma_6) + \frac{1}{2} \delta_i (\pi_{2z} + \pi_{3z} + \pi_{4z} + \pi_{5z}) + \frac{1}{2} \epsilon_i (\pi_{2y} + \pi_{3x} - \pi_{4y} - \pi_{5x}), \\ \Psi_{x^2-y^2} &= \alpha' d_{x^2-y^2} + \frac{1}{2} \xi_i (s_2 - s_3 + s_4 - s_5) + \frac{1}{2} \kappa_i (\sigma_2 - \sigma_3 + \sigma_4 - \sigma_5), \\ \Psi_{3z^2-r^2} &= \alpha' d_{3z^2-r^2} + \frac{1}{2\sqrt{3}} \xi_i (2s_1 - s_2 - s_3 - s_4 - s_5 + 2s_6) + \frac{1}{2\sqrt{3}} \kappa_i (2\sigma_1 - \sigma_2 - \sigma_3 - \sigma_4 - \sigma_5 + 2\sigma_6). \end{aligned} \quad (10)$$

The definition of the orbitals is depicted in Fig. 8(b). Using Eqs. (5) and (6) one obtains, for the matrix elements,

$$\begin{aligned} B_{xx} = B_{yy} &= \frac{1}{2S} \frac{1}{4} [\delta_i^2 + \epsilon_i^2 - 2(\gamma_i^2 + \frac{2}{3}\kappa_i^2)] b \\ &\quad - \frac{1}{2S} (3\alpha^2 + 2\alpha'^2) b_{dd}, \\ B_{zz} &= -B_{xx} - B_{yy}, \\ B_{xy} = B_{yx} &= \frac{1}{2S} \frac{3}{2} \delta_i \epsilon_i b, \\ B_{xz} = B_{zx} = B_{yz} = B_{zy} &= 0. \end{aligned} \quad (11)$$

For the Fermi-contact interaction one obtains

$$a_i = \frac{1}{2S} (\frac{1}{2}\beta_i^2 + \frac{1}{3}\xi_i^2) \frac{2}{3} \mu_0 g \mu_B g_N \mu_N |s(0)|^2. \quad (12)$$

The transferred spin density to shell i equals

$$\frac{3}{5} (\beta_i^2 + \gamma_i^2 + \delta_i^2 + \epsilon_i^2) + \frac{2}{5} (\xi_i^2 + \kappa_i^2)$$

and can neither be calculated. Again, it is impossible to discriminate between contributions from the σ orbitals of the t_2 and e states when $B_{xx} > 0$. Nor is it possible to discriminate between the contributions from the s orbitals of the t_2 and e states.

For the class-M shell tensors it is convenient to calculate them in a $\pi_x \pi_y \sigma$ coordinate system. The choice of the orbitals is shown in Fig. 8(c). The wave functions are

$$\begin{aligned} \Psi_{yz} &= ad_{yz} + \frac{1}{2} \beta_i (-s_5 + s_6 - s_{11} + s_{12}) + \frac{1}{2\sqrt{2}} \gamma_i (s_1 - s_2 - s_3 - s_4 - s_7 + s_8 + s_9 + s_{10}) + \frac{1}{2} \delta_i (-\sigma_5 + \sigma_6 - \sigma_{11} + \sigma_{12}) \\ &\quad + \frac{1}{2\sqrt{2}} \epsilon_i (\sigma_1 - \sigma_2 - \sigma_3 - \sigma_4 - \sigma_7 + \sigma_8 + \sigma_9 + \sigma_{10}) + \frac{1}{2\sqrt{2}} \xi_i (\pi_{1x} - \pi_{2x} + \pi_{3x} + \pi_{4x} - \pi_{7x} + \pi_{8x} - \pi_{9x} - \pi_{10x}) \\ &\quad + \frac{1}{2\sqrt{2}} \kappa_i (\pi_{1y} - \pi_{2y} - \pi_{3y} - \pi_{4y} - \pi_{7y} + \pi_{8y} + \pi_{9y} + \pi_{10y}) + \frac{1}{2} \lambda_i (-\pi_{5y} + \pi_{6y} - \pi_{11y} + \pi_{12y}), \\ \Psi_{zx} &= ad_{zx} + \frac{1}{2} \beta_i (s_3 - s_4 + s_9 - s_{10}) + \frac{1}{2\sqrt{2}} \gamma_i (-s_1 - s_2 + s_5 + s_6 + s_7 + s_8 - s_{11} - s_{12}) + \frac{1}{2} \delta_i (\sigma_3 - \sigma_4 + \sigma_9 - \sigma_{10}) \\ &\quad + \frac{1}{2\sqrt{2}} \epsilon_i (-\sigma_1 - \sigma_2 + \sigma_5 + \sigma_6 + \sigma_7 + \sigma_8 - \sigma_{11} - \sigma_{12}) + \frac{1}{2\sqrt{2}} \xi_i (\pi_{1x} + \pi_{2x} + \pi_{5x} + \pi_{6x} - \pi_{7x} - \pi_{8x} - \pi_{11x} - \pi_{12x}) \\ &\quad + \frac{1}{2\sqrt{2}} \kappa_i (-\pi_{1y} - \pi_{2y} + \pi_{5y} + \pi_{6y} + \pi_{7y} + \pi_{8y} - \pi_{11y} - \pi_{12y}) + \frac{1}{2} \lambda_i (\pi_{3y} - \pi_{4y} + \pi_{9y} - \pi_{10y}), \end{aligned}$$

$$\begin{aligned} \Psi_{xy} = & \alpha d_{xy} + \frac{1}{2} \beta_i (s_1 - s_2 + s_7 - s_8) + \frac{1}{2\sqrt{2}} \gamma_i (s_3 - s_4 + s_5 - s_6 - s_9 + s_{10} - s_{11} + s_{12}) + \frac{1}{2} \delta_i (\sigma_1 - \sigma_2 + \sigma_7 - \sigma_8) \\ & + \frac{1}{2\sqrt{2}} \epsilon_i (\sigma_3 - \sigma_4 + \sigma_5 - \sigma_6 - \sigma_9 + \sigma_{10} - \sigma_{11} + \sigma_{12}) + \frac{1}{2\sqrt{2}} \xi_i (\pi_{3x} - \pi_{4x} - \pi_{5x} + \pi_{6x} - \pi_{9x} + \pi_{10x} + \pi_{11x} - \pi_{12x}) \\ & + \frac{1}{2\sqrt{2}} \kappa_i (\pi_{3y} - \pi_{4y} + \pi_{5y} - \pi_{6y} - \pi_{9y} + \pi_{10y} - \pi_{11y} + \pi_{12y}) + \frac{1}{2} \lambda_i (\pi_{1y} - \pi_{2y} + \pi_{7y} - \pi_{8y}), \end{aligned} \quad (13)$$

$$\begin{aligned} \Psi_{x^2-y^2} = & \alpha' d_{x^2-y^2} + \frac{1}{2\sqrt{2}} \mu_i (-s_3 - s_4 + s_5 + s_6 - s_9 - s_{10} + s_{11} + s_{12}) \\ & + \frac{1}{2\sqrt{2}} \xi_i (-\sigma_3 - \sigma_4 + \sigma_5 + \sigma_6 - \sigma_9 - \sigma_{10} + \sigma_{11} + \sigma_{12}) + \frac{1}{2\sqrt{2}} \rho_i (-\pi_{3y} - \pi_{4y} + \pi_{5y} + \pi_{6y} - \pi_{9y} - \pi_{10y} + \pi_{11y} + \pi_{12y}) \\ & + \frac{1}{2\sqrt{6}} \tau_i (2\pi_{1x} + 2\pi_{2x} - \pi_{3x} - \pi_{4x} - \pi_{5x} - \pi_{6x} + 2\pi_{7x} + 2\pi_{8x} - \pi_{9x} - \pi_{10x} - \pi_{11x} - \pi_{12x}), \end{aligned}$$

$$\begin{aligned} \Psi_{3z^2-r^2} = & \alpha' d_{3z^2-r^2} + \frac{1}{2\sqrt{6}} \mu_i (2s_1 + 2s_2 - s_3 - s_4 - s_5 - s_6 + 2s_7 + 2s_8 - s_9 - s_{10} - s_{11} - s_{12}) \\ & + \frac{1}{2\sqrt{6}} \xi_i (2\sigma_1 + 2\sigma_2 - \sigma_3 - \sigma_4 - \sigma_5 - \sigma_6 + 2\sigma_7 + 2\sigma_8 - \sigma_9 - \sigma_{10} - \sigma_{11} - \sigma_{12}) \\ & + \frac{1}{2\sqrt{6}} \rho_i (2\pi_{1y} + 2\pi_{2y} - \pi_{3y} - \pi_{4y} - \pi_{5y} - \pi_{6y} + 2\pi_{7y} + 2\pi_{8y} - \pi_{9y} - \pi_{10y} - \pi_{11y} - \pi_{12y}) \\ & + \frac{1}{2\sqrt{2}} \tau_i (\pi_{3x} + \pi_{4x} - \pi_{5x} - \pi_{6x} + \pi_{9x} + \pi_{10x} - \pi_{11x} - \pi_{12x}). \end{aligned}$$

Using Eqs. (5) and (6), the following matrix elements are obtained:

$$\begin{aligned} B_{\xi\xi} &= \frac{1}{2S} \left(-\frac{1}{4} \delta_i^2 - \frac{1}{4} \lambda_i^2 - \frac{1}{4} \epsilon_i^2 + \frac{1}{2} \xi_i^2 - \frac{1}{4} \kappa_i^2 + \frac{1}{3} \tau_i^2 - \frac{1}{6} \xi_i^2 - \frac{1}{6} \rho_i^2 \right) b - \frac{1}{2S} (3\alpha^2 + 2\alpha'^2) b_{dd}, \\ B_{\eta\eta} &= \frac{1}{2S} \left(-\frac{1}{4} \delta_i^2 + \frac{1}{2} \lambda_i^2 - \frac{1}{4} \epsilon_i^2 - \frac{1}{4} \xi_i^2 + \frac{1}{2} \kappa_i^2 - \frac{1}{6} \tau_i^2 - \frac{1}{6} \xi_i^2 + \frac{1}{3} \rho_i^2 \right) b - \frac{1}{2S} (3\alpha^2 + 2\alpha'^2) b_{dd}, \\ B_{\xi\xi} &= \frac{1}{2S} \left(+\frac{1}{2} \delta_i^2 - \frac{1}{4} \lambda_i^2 + \frac{1}{2} \epsilon_i^2 - \frac{1}{4} \xi_i^2 - \frac{1}{4} \kappa_i^2 - \frac{1}{6} \tau_i^2 + \frac{1}{3} \xi_i^2 - \frac{1}{6} \rho_i^2 \right) b + \frac{1}{S} (3\alpha^2 + 2\alpha'^2) b_{dd}, \\ B_{\eta\xi} &= B_{\xi\eta} = \frac{1}{2S} \frac{3}{4} (\delta_i \lambda_i + \epsilon_i \kappa_i + \frac{2}{3} \xi_i \rho_i) b, \\ B_{\xi\eta} &= B_{\eta\xi} = B_{\xi\xi} = B_{\xi\xi} = 0. \end{aligned} \quad (14)$$

The Fermi-contact interactions read

$$a_i = \frac{1}{2S} \frac{1}{4} (\beta_i^2 + \gamma_i^2 + \frac{2}{3} \mu_i^2) \frac{2}{3} \mu_0 g \mu_B g_N \mu_N |s(0)|^2. \quad (15)$$

For a class-G tensor the expressions for the wave functions Ψ are again lengthier than for the class-M tensors. The expression for the Fermi-contact interaction contains five parameters and the expressions for the matrix elements B_{ij} contain 15 parameters. The two class-G tensors do not give a significant contribution to the MTSD as the measured hyperfine interactions with the two shells are rather small. Therefore we will only give the results of the calculated MTSD for these two shells.

In Table II are given the calculated Fermi-contact interactions and the derived values of the transferred spin to the ligand s orbitals. For the tensors T1 and 33 no numbers for the spin density are given because the positive values of the contact interaction cannot be analyzed

TABLE II. Parameters for the isotropic hyperfine contact interaction, a , for the ^{29}Si neighbors of Cr_i^+ , and derived transfer of spin density to ligand s orbitals, per shell. Spin densities for the tensors 33 and T1 could not be calculated because positive contact interactions are inconsistent with Eqs. (8) and (12), respectively.

Tensor	a (kHz)	Transfer of spin density (%)
G1	-612.3	0.32
G2	-167.8	0.09
M1	-2359.2	0.62
M2	-1387.5	0.37
M3	-506.9	0.13
31	-5067.4	0.45
32	-3269.3	0.29
33	+216.7	
T1	+668.3	

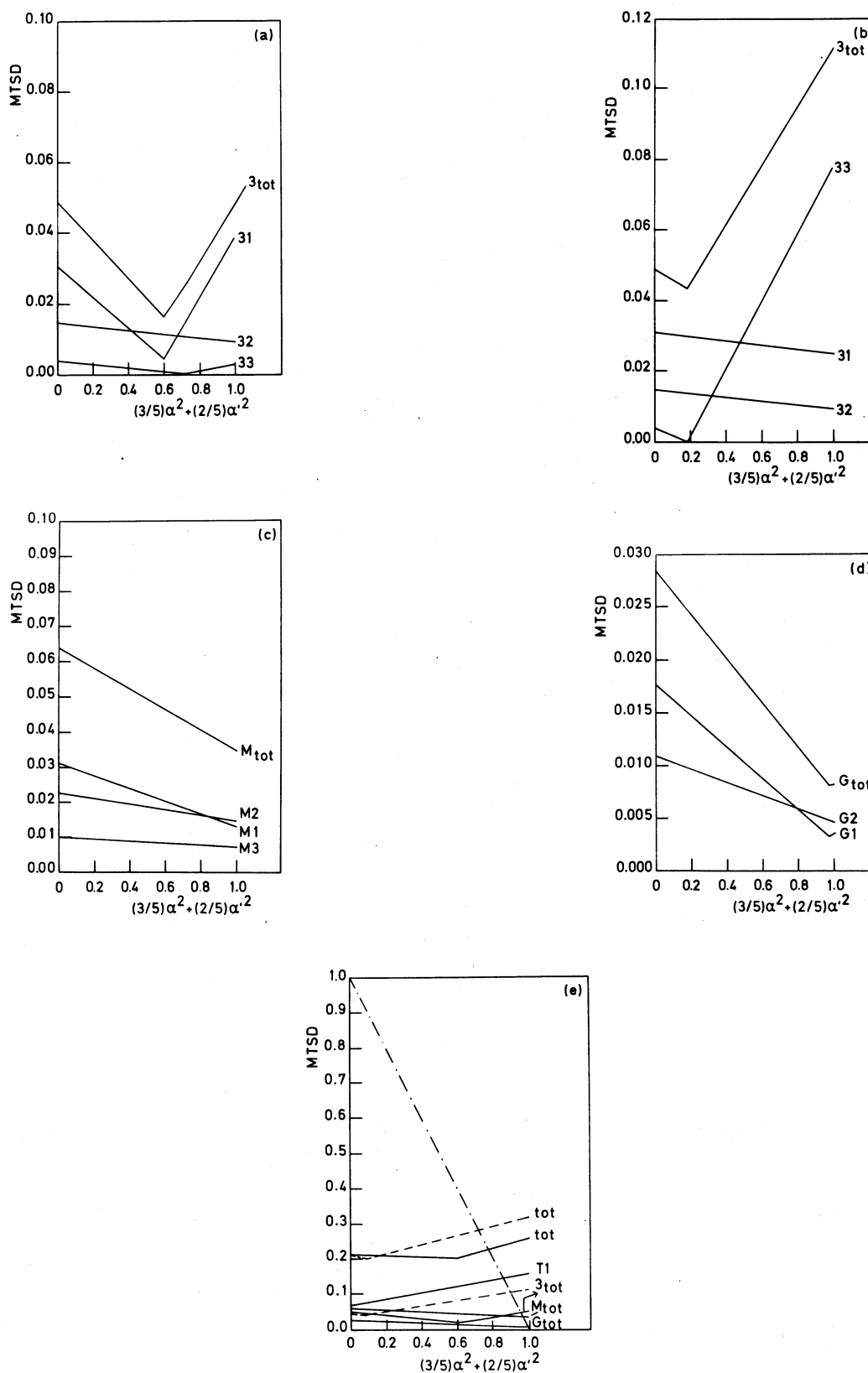


FIG. 9. (a) Minimum transfer of spin density (MTSD) for the class-3 tensors as a function of the localization ($\frac{3}{5}\alpha^2 + \frac{2}{5}\alpha'^2$) on the impurity atom in lattice-site assignment 1 of Table III. Transfer to σ orbitals predominates. (b) MTSD for the class-3 tensors as a function of the localization ($\frac{3}{5}\alpha^2 + \frac{2}{5}\alpha'^2$) on the impurity atom in lattice-site assignment 2 of Table III. Transfer to π orbitals predominates. (c) MTSD as a function of the localization ($\frac{3}{5}\alpha^2 + \frac{2}{5}\alpha'^2$) on the impurity atom, for the class-M tensors. (d) MTSD as a function of the localization ($\frac{3}{5}\alpha^2 + \frac{2}{5}\alpha'^2$) on the impurity atom, for the class-G tensors. (e) MTSD as a function of the localization ($\frac{3}{5}\alpha^2 + \frac{2}{5}\alpha'^2$) on the impurity atom for the 2mm-class tensor and the total MTSD for all nine shells. The solid and dashed lines refer to assignments 1 and 2 of Table III, respectively.

TABLE III. Assignment of experimental tensors to atomic sites around the Cr_i^+ impurity. For the class-M shells tensors are given the angles between the direction of the largest principal values and lattice vectors. For the class-G tensors are given the angles between the lattice vectors and the directions of the second largest principal value for G1 and the smallest principal value for G2.

Tensor	Atom lmn	Axis	Angle with $[lmn]$ (deg)
G1	204	[0.545, -0.152, 0.824]	11.3
G2	$\bar{3}\bar{5}1$	[0.587, -0.804, 0.100]	6.2
M1	$\bar{1}\bar{1}\bar{3}$	[0.433, 0.433, 0.791]	12.4
M2	331	[0.672, 0.672, 0.313]	4.6
M3	442	[0.603, 0.603, 0.523]	11.9

	Assignment 1	Assignment 2
31	111	222 or $\bar{2}\bar{2}\bar{2}$
32	222 or $\bar{2}\bar{2}\bar{2}$	$\bar{2}\bar{2}\bar{2}$ or 222
33	$\bar{2}\bar{2}\bar{2}$ or 222	111
T1	002 or $00\bar{2}$	

using Eqs. (12) and (8).

In order to derive the minimum transfer of spin density for the p part of the wave functions, the measured hyperfine interactions are corrected for the dipole-dipole contributions from the electron-spin density on the Cr ion. These corrections are calculated in a point-charge approximation. The dipole-dipole contributions can only be calculated when the experimental tensors are assigned to specific lattice sites (shells). In the analysis the MTSD to the silicon atoms is then calculated as a function of the density $\frac{2}{3}\alpha^2 + \frac{2}{5}\alpha'^2$ on the impurity. As the contribution from the distant dipole-dipole interaction can be of considerable magnitude, a different assignment of tensors to shells can significantly alter the interpretation of the experimental data.

The only hyperfine tensor which can be assigned with certainty to a specific shell of atoms is T1. The six atoms in this shell are the next-nearest neighbors to the impurity. Using the expressions Eqs. (11) the MTSD is calculated, the result of which is shown in Fig. 9(e). The experimental observation that this tensor is nearly axial around the [110] direction makes it comparable to the tensor T1 that was measured for Ti_i^+ . In the case of Ti_i^+ ($3d^3$, electronic configuration t_2^3), the admixture of σ orbitals, although formally allowed, is yet suppressed by symmetry reasons.¹⁶ For Cr_i^+ ($3d^5$, configuration $t_2^3e^2$), also a certain admixture of σ orbitals from the e state would be expected. This would then be comparable to the case of Fe_i^0 ($3d^8$, configuration e^2), where, by symmetry, the transfer of spin density to π orbitals is forbidden, and a $\langle 100 \rangle$ axial tensor would be expected; in experiment the tensor T1 for Fe_i^0 is nearly $\langle 100 \rangle$ axial indeed.¹⁵ The conclusion that can be drawn from above considerations is that Cr_i^+ is very similar to Ti_i^+ regarding the hybridization of the t_2 electrons of the impurity with the next-nearest-neighbor ligand π orbitals, while the e electrons hardly hybridize with the σ orbitals.

For the other three types of shells it is not possible to assign hyperfine-interaction tensors to specific shells of atoms in an unambiguous way. A usually adopted method is to assign the tensor with the largest isotropic hyperfine interaction to the nearest shell of atoms, the tensor with the second-largest interaction to the second-nearest-neighbor shell, and so on. One should be well aware, however, that such a strategy is not supported by a solid knowledge of the electronic structure of the impurity; it is mainly an intuitive choice. The assignment of tensors to lattice sites can give rather different values for the MTSD depending on the choice that is made in this respect, as will be illustrated for the class-3 shells. The physical interpretation will be, in general, quite different, depending on the choice.

In Fig. 9(a) the MTSD for the three class-3 tensors is shown as calculated for the assignment to shells according to monotonously decreasing values of the Fermi-contact hyperfine interaction in the sequence 31, 32, 33 (see Table III). Alternatively, the assignment of tensor 33 with shell 1 (sites 111), tensor 32 with shell 4 or shell 5 (sites 222 or $\bar{2}\bar{2}\bar{2}$, respectively), and tensor 31 with shell 5 or shell 4, was considered. Results are illustrated in Fig. 9(b). The picture changes dramatically depending especially on the assignment of tensor 33. In the alternative assignment it is assumed that the isotropic part of the hyperfine interaction need not be an indicator of distance to the impurity, as both admixture and exchange polarization may contribute.

In assigning the experimental tensors to lattice sites for the class-M shells, we used the same procedure as in the case of Ti_i^+ , i.e., we choose nearby lattice sites in the $(\bar{1}10)$ plane that make a small angle with the direction of the largest principal value of the experimental tensor. In Fig. 10 the principal directions with the largest value for the three class-M tensors are shown. They all lie in the $(\bar{1}10)$ plane. In Table III the lattice sites that were assigned to them are given. In the case of ti-

TABLE IV. Experimental values for the (minimum) spin transfer, theoretical values for the reduction of the magnetic moment α^2 , and experimental and theoretical values for the reduction of the central ion hyperfine interaction λ . Values $1-\alpha^2$ and $1-\lambda$ are given to allow direct comparison with the first column.

Transition metal	Spin transfer (Experiment ^{29}Si)	$1-\alpha^2$		$1-\lambda$	
		(Ref. 14)	(Ref. 12)	(Expt.)	(Refs. 8, 11)
Cr_i^+	> 0.22	0.34	0.25	0.54	0.53
Ti_i^+	> 0.40	0.58	0.33	0.75	0.78
Fe_i^0	0.25	0.12	0.29	0.54	0.66

tanium this choice seemed justified because all the observed tensors fell within 10° of the directions to specific lattice sites in the $(\bar{1}10)$ plane, indicating a predominant admixture of σ orbitals. For chromium this choice cannot be substantiated as there are only three class-M tensors, one of which is also nearly $\langle 111 \rangle$ axial. Still this choice is not unreasonable in regard to the earlier-noted similarities between the two impurities. The resulting MTSD as a function of the localization $\frac{3}{5}\alpha^2 + \frac{2}{5}\alpha'^2$ on the impurity is plotted in Fig. 9(c).

For the class-G tensors we looked for nearby lattice sites whose directions had a small deviation from one of the three principal directions of the tensor. This resulted in assigning G1 to site 204 and G2 to site 351. This means that just as for the class-M shells the admixture of σ orbitals predominates, in contrast with the class-G shells for Ti_i^+ , which are all nearly $\langle 111 \rangle$ axial. These assignments have to be considered tentative. We did not pursue other possible choices as these two tensors contribute at most about 2%, irrespective of the assignment that is made. Resulting values for the MTSD are shown in Fig. 9(d).

Addition of all the contributions from the different shells yields the solid line labeled "tot" in Fig. 9(e). This line intersects the line $\mathcal{D}_{\min} = 1 - (\frac{3}{5}\alpha^2 + \frac{2}{5}\alpha'^2)$ at $\mathcal{D}_{\min} = 0.224$ (with assignment 1 for the class-3 tensors). This means that the transferred spin density to the crystal is at least 22.4% (or that the spin density localized on the impurity is at most 77.6%). From the reduction of the core polarization of the impurity, an upper limit to the MTSD was estimated to be 52%. The MTSD for assignment 2 to the class-3 tensors is about 28%.

In Table IV these experimental results and those for Ti_i^+ and Fe_i^0 are compared with theoretical calculations.²³ The second column gives the values for the (minimum) spin density transferred to the ligand atoms calculated from the experimentally determined hyperfine-interaction tensor parameters using the method described in this article. In the third column are given theoretical numbers as calculated by Katayama-Yoshida and Zunger,^{12,24} and by Beeler *et al.*¹⁴ The first authors calculated the local magnetic moment for a transition-metal impurity in a certain impurity orbital subspace, designated Δm . The total magnetic moment in the whole space is $\Delta M = 2S$. The quantity $1-\alpha^2 = 1 - \Delta m / \Delta M$ as a measure for the delocalization of the impurity wave function through the crystal is given in the column below Ref. 12. The second group of authors calculated the spin density m_0 in an impurity

atomic sphere (muffin tin). The delocalization is now defined as $1-\alpha^2 = 1 - m_0/m$, where m is the total spin density of crystal plus impurity. These values are given in the column below Ref. 14. The differences between the values found by the two groups are quite large. Causes can be sought in differences in the computational techniques used. First, the extent of the impurity space can be quite different as a result of the different methods and definitions. Another important difference is that Beeler *et al.* used a frozen-core approximation and could not calculate the self-interaction hyperfine constant, which is the sum of spin densities from core and valence s orbitals. Experimentally, a marked difference in localization between e orbitals (Fe_i^0) and t_2 orbitals is found. Qualitatively, this is overestimated by Beeler's results¹⁴ and somewhat underestimated by Katayama-Yoshida and Zunger.^{12,24} The last two columns of Table IV give the reduction of the central hyperfine interaction, which is defined as $\lambda = A_{\text{exp}}/A_{\text{free ion}}$. Given values are ratios of either experimentally measured impurity hyperfine interactions³ or calculated ones by Katayama-Yoshida and Zunger¹¹ and free-ion or atom hyperfine fields as given by Watson and Freeman.⁸ As can be seen, agreement is very good. We would like to stress

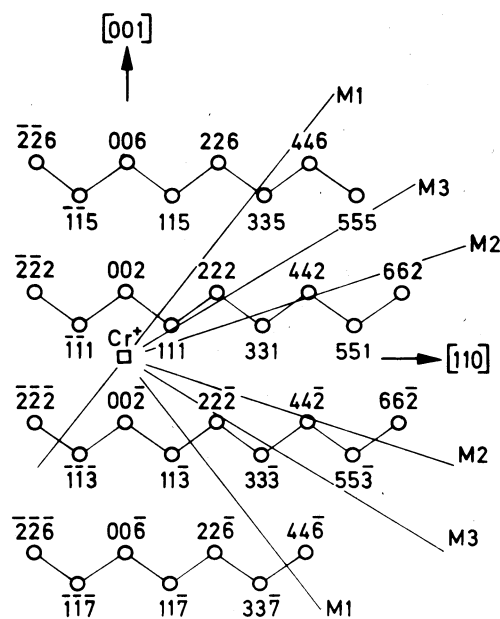


FIG. 10. Directions of the largest principal values of the three mirror-plane-class tensors in the $(\bar{1}10)$ plane.

TABLE V. Experimental hyperfine parameters for the five nearest-neighbor shells of silicon atoms for interstitial Fe^0 , Ti^+ , and Cr^+ , and theoretically calculated contact terms for the five nearest-neighbor shells of silicon atoms around Fe^0 . Units are kHz.

Shell	Atom no.	Fe_i^0		Ti_i^+	Cr_i^+
		Expt. a	Theor. a		
3(111)	1	+ 158	+ 150	- 8124	- 5067
3(222)	4	+ 777	+ 670	- 1417	- 3269
$3(\bar{2}\bar{2}\bar{2})$	5	+ 3245	+ 2790	- 749	+ 217
T(200)	2	- 4642	- 16 660	- 852	+ 668
M(113)	3	- 3870	- 3700	- 2246	- 2359

that the numbers given in the second column of Table IV refer to values that were derived from measurements of the spin density on the ligand atoms, while the numbers in the other columns refer to values obtained from measurements and calculations regarding the transition-metal impurity. In fact, the sums (spin transfer) $+\alpha^2$ and (spin transfer) $+\lambda$ should be 1.

Only very recently have results of theoretical calculations of the magnitude and sign of contact interactions of silicon ligand nuclei for $\text{Si}:\text{Fe}_i^0$ become available.^{25,26} In Table V these numbers are given together with the experimentally determined values for the three transition metals that have been investigated with ENDOR. The computational method which was used was an *ab initio* supercell full-potential linearized augmented-plane-wave (FLAPW) method. The supercell which was used by Katayama-Yoshida and Hamada consisted of a cubic unit cell with the Fe atom in the center, surrounded by eight silicon atoms just as in Fig. 5. Because of this small cluster only three "shells" of atoms exist. As a result of periodic boundary conditions, atoms can be neighbors of several impurity ions at the same time. Atoms of shell Si(I) are at position 1 of the nearest ion, while at the same time at position 3 with respect to three other ions. The calculated hyperfine contact term for this shell is thus actually a sum: $a^{\text{calc}}(\text{I})=1\times a^{\text{calc}}(1)+3\times a^{\text{calc}}(3)$. Similarly, atoms of shell Si(II) are at position 2 with respect to two ions at the same time: $a^{\text{calc}}(\text{II})=2\times a^{\text{calc}}(2)$. Atoms of shell Si(III) are at position 4 with respect to four and at position 5 with respect to another four ions: $a^{\text{calc}}(\text{III})=4\times a^{\text{calc}}(4)+4\times a^{\text{calc}}(5)$. The individual contributions are next calculated under the assumption

$$\frac{a^{\text{calc}}(i)}{a^{\text{calc}}(j)} = \frac{a^{\text{expt}}(i)}{a^{\text{expt}}(j)}$$

In Table V the sign of $a[3(111)]$ and the magnitude of $a[M(113)]$ have been changed with respect to Ref. 25 because the authors used the experimental hyperfine parameters as given by Greulich-Weber *et al.*,¹⁵ who did not determine the sign of the hyperfine parameters and chose $a[3(111)]<0$, while it was later found to be positive.¹⁷ It should be noted that, when directly applying the method as outlined above to the spin-density values

in Ref. 25, we actually arrive at calculated hyperfine values a which are a factor of $\frac{3}{4}$ smaller than those given in Ref. 25 and as reproduced in Table V. Although the size of the unit cell seems rather unrealistic, the calculated and measured values, except for T(200), are in surprisingly good agreement. The large discrepancy for T(200) is attributed by the authors to an artifact of the small size of the cluster.

The sign of the contact interactions can qualitatively be understood as follows. For the class-3 shells the impurity e states cannot couple with the silicon s orbitals. Although for Fe_i^0 the t_2 state is fully occupied, there still is a spin density at the ligand nuclei because the spin-up spin densities are slightly more localized than the spin-down spin densities. Therefore, Katayama-Yoshida and Hamada^{25,26} conclude that the resulting spin density will be positive at the nearest-neighbor shell, giving a small negative a as g_N is negative for silicon. At the shells 4 and 5 the net spin density will be negative, resulting in a positive a . Although the authors claim that this is also observed experimentally, the nearest-neighbor shell has, in fact, a positive a . This suggests that the spin-up spin density is even more contracted towards the iron impurity, so that even the nearest neighbors are already in the spin-down tail. In the case of Ti^+ and Cr^+ , admixture of silicon s orbitals is allowed and results in (large) negative values for a . The (small) positive value of a for shell $3(\bar{2}\bar{2}\bar{2})$ of Cr^+ indicates a competition between the negative contributions from silicon $3s$ orbitals and positive contributions from silicon core orbitals. In the case of the T(200) tensor there is a clear difference between Fe_i^0 on one side and Ti_i^+ and Cr_i^+ on the other. Whereas for Fe a is large and negative, for Ti^+ and Cr^+ the contact terms are small. These observations comply very well with the fact that for e states admixture of s orbitals is allowed. Although in t_2 states s admixture is formally also allowed, in the case of Ti^+ and Cr^+ it is found that admixture of s orbitals does not occur. One might expect that for Cr^+ a would be more negative than for Ti^+ , because for Cr^+ extra admixture from e states would be expected. This is obviously not the case as the contact term of Cr^+ is even positive. The large overall similarity between Cr_i^+ ($t_2^3e^2$) and Ti_i^+ (t_2^3) and the differences with Fe_i^0 (e^2) demonstrate that the chromium e states are much less delocalized than the t_2 states. For the mir-

rorplane class tensors of Fe_i^0 , Ti_i^+ , and Cr_i^+ , admixture of s , σ , π_x , and π_y orbitals is allowed. The large negative values of a for all three impurities indicate a considerable admixture of s orbitals.

V. CONCLUSIONS

In an ENDOR experiment we determined the hyperfine interaction between the electrons of the singly positively charged state of interstitial chromium in silicon with nine shells of silicon neighbors comprising 102 atoms. Using an analysis that takes into account all five valence electrons of the impurity and the symmetry

properties of the impurity in the host crystal, it was possible to eliminate the apparent contradiction between the large reduction of the core polarization of the impurity and the absence of any large hyperfine interactions with the ligand nuclei. This analysis alone could not account for the positive sign of the hyperfine parameter a which occurred for two neighbor shells of silicon atoms.

ACKNOWLEDGMENT

This work received financial support from the Foundation for Fundamental Research on Matter (FOM), The Netherlands.

-
- ¹H. H. Woodbury and G. W. Ludwig, *Phys. Rev.* **117**, 102 (1960).
²H. H. Woodbury and G. W. Ludwig, *Phys. Rev. Lett.* **5**, 96 (1960).
³G. W. Ludwig and H. H. Woodbury, in *Solid State Physics*, edited by F. Seitz and D. Turnbull (Academic, New York, 1962), Vol. 13, p. 223.
⁴D. A. van Wezep and C. A. J. Ammerlaan, *J. Electron. Mater.* **14a**, 863 (1985).
⁵E. R. Weber, *Appl. Phys. A* **30**, 1 (1983).
⁶H. Feichtinger and R. Czaputa, *Appl. Phys. Lett.* **39**, 706 (1981).
⁷H. Conzelmann, K. Graff, and E. R. Weber, *Appl. Phys. A* **30**, 169 (1983).
⁸R. E. Watson and A. J. Freeman, in *Hyperfine Interactions*, edited by A. J. Freeman and R. B. Frankel (Academic, New York, 1967), p. 53.
⁹H. Katayama-Yoshida and A. Zunger, *Phys. Rev. Lett.* **53**, 1256 (1984).
¹⁰H. Katayama-Yoshida and A. Zunger, *Phys. Rev. B* **31**, 7877 (1985).
¹¹H. Katayama-Yoshida and A. Zunger, *Phys. Rev. B* **31**, 8317 (1985).
¹²A. Zunger, in *Solid State Physics*, edited by H. Ehrenreich and D. Turnbull (Academic, Orlando, 1986), Vol. 39, p. 275.
¹³F. Beeler, O. K. Andersen, and M. Scheffler, *Mater. Res. Soc. Symp. Proc.* **46**, 129 (1985).
¹⁴F. Beeler, O. K. Andersen, and M. Scheffler, *Phys. Rev. Lett.* **55**, 1498 (1985).
¹⁵S. Greulich-Weber, J. R. Niklas, E. R. Weber, and J. M. Spaeth, *Phys. Rev. B* **30**, 6292 (1984).
¹⁶D. A. van Wezep, R. van Kemp, E. G. Sieverts, and C. A. J. Ammerlaan, *Phys. Rev. B* **32**, 7129 (1985).
¹⁷D. A. van Wezep, T. Gregorkiewicz, E. G. Sieverts, and C. A. J. Ammerlaan, *Phys. Rev. B* **34**, 4511 (1986).
¹⁸F. V. Strnisa and J. W. Corbett, *Cryst. Lattice Defects* **5**, 261 (1974).
¹⁹G. H. Fuller, *J. Phys. Chem. Ref. Data* **5**, 835 (1976).
²⁰G. D. Watkins and J. W. Corbett, *Phys. Rev.* **134**, A1359 (1964).
²¹J. Owen and J. H. M. Thornley, *Rep. Progr. Phys. (G.B.)* **29**, 675 (1966).
²²J. R. Morton and K. F. Preston, *J. Magn. Reson.* **30**, 577 (1978).
²³E. G. Sieverts, D. A. van Wezep, R. van Kemp, and C. A. J. Ammerlaan, *Mater. Sci. Forum* **10-12**, 729 (1986).
²⁴H. Katayama-Yoshida and A. Zunger, *Phys. Rev. Lett.* **55**, 1618 (1985).
²⁵H. Katayama-Yoshida and N. Hamada, *Mater. Sci. Forum* **10-12**, 61 (1986).
²⁶H. Katayama-Yoshida and N. Hamada, *Phys. Rev. B* **35**, 407 (1987).